LA-UR- 09-01168

Approved for public release; distribution is unlimited.

Title: Ion Heating and energy partition at the heliospheric termination shock: Hybrid simulations and analytical model

Author(s): S. Peter Gary, 082438, ISR-1, LANL
Pin Wu, Boston University
Dan Winske, 082493, X-1, LANL
N. A. Schwadron, Boston University
M. Lee, University of New Hampshire

Intended for: Journal of Geophysical Research

Los Alamos NATIONAL LABORATORY EST. 1943

Ion Heating and energy partition at the heliospheric termination shock: Hybrid simulations and analytical model

P. Wu,[1,2] D. Winske,[1] S. P. Gary,[1] N. A. Schwadron,[2] M. Lee[3]

P. Wu, N. A. Schwadron, Department of Astronomy, Boston University, 725 Commonwealth Ave., Boston, MA 02215, USA. (nanopenny@gmail.com, nathanas@bu.edu)

D. Winske, S. P. Gary, Mail Stop D466, Group ISR-1, Los Alamos National Laboratory, Los Alamos, NM 87545. (winske@lanl.gov, pgary@lanl.gov)

[1]Los Alamos National Laboratory, Los Alamos, New Mexico, USA.

[2]Department of Astronomy, Boston University, Massachusetts, USA.

[3]Department of Physics, University of New Hampshire, New Hampshire, USA.

Abstract. We use the one dimensional Los Alamos hybrid simulation code to examine heating and energy dissipation at the perpendicular heliospheric termination shock in the presence of pickup ions (PUIs). The simulations are 1D in space but 3D in field and velocity components, and are carried out for a range of values of the pickup ion relative density. The simulations show that, because they are relatively cold upstream, the solar wind ions have a relatively large temperature gain across the shock. But, as the relative pickup ion density is increased, the pickup ions gain the larger share of the downstream pressure, consistent with Voyager 2 observations at the termination shock. An analytic model for energy partition among the transmitted solar wind ions, the reflected solar wind ions, and the pickup ions is developed for the perpendicular termination shock. Results of this model are consistent with both hybrid simulations and the Voyager 2 observations.

1. Introduction

The heliospheric termination shock marks the heliospheric boundary, where the solar wind makes its transition from supersonic to subsonic flow. It is believed to be quasi-perpendicular at most heliospheric latitudes because of the shock's great distance from the Sun and the Parker spiral structure of the heliospheric magnetic field.

Voyager 1 (V1) crossed the termination shock in December 2004 at the heliocentric distance of 94 AU and a heliospheric latitude of 34.1° [*Stone et al.*, 2005]. In August 2007 Voyager 2 (V2) crossed the termination shock at 84 AU and a heliographic latitude L of -27.5° [*Decker et al.*, 2008]. At the times of their respective crossings, both V1 and V2 carried operating magnetometers, but only V2 carried a functional plasma instrument. Thus, as the summary of observations in Table 1 shows, V2 provided the more complete set of plasma and field measurements.

The upstream plasma is thought to consist of two distinct ion components: the thermal solar wind component with T $\approx$ 1 eV, as observed by V2, and a pickup ion component with an average energy about 1 keV. The plasma instrument on Voyager 2 measured the few eV thermal ion component near the shock and into the heliosheath, but neither Voyager was able to directly observe the few keV pickup ions. Both the solar wind and the pickup ions are heated at the termination shock, but there is substantial disagreement about the relative energy gain of the two. *Zank et al.* [1996] show that pickup ions are more likely to be reflected at the termination shock and gain more energy than the solar wind ions. *Richardson et al.* [2008] reported that solar wind ions only account for 20% of the heating based on V2 observations. They postulated that pick-up ions (PUIs) account for the rest of heating. However, *Liewer et al.* [1993] reported that even with 20% of the solar wind density in the form of pickup hydrogen, their 1D hybrid simulations showed that the solar wind ions provide most of the dissipation. Our study uses the Los Alamos hybrid simulation code to determine the relative heating of solar wind and pick-up ions at a model termination shock to understand why there is a discrepancy between these two points of view. Another puzzle the v2 observations raise is that the downstream flow remains supersonic with respect to the thermal ions [*Li et al.*, 2008].

Consider quasi-perpendicular shocks with a single, relatively cold, upstream ion component. In such shocks above the critical Mach number M_c [*Woods*, 1969], ion reflection is a well known phenomena confirmed by hybrid simulations [e.g., *Quest*, 1985; *Gosling and Robson*, 1985; *Goodrich*, 1985; *Winske et al.*, 1986], laboratory studies [e.g., *Phillips and Robson*, 1972] and spacecraft observations of Earth's bow shock [e.g., *Paschmann et al.*, 1982; *Sckopke et al.*, 1983]. Adiabatic heating and anomalous resistivity are not sufficient to account for energy dissipation across the shock [e.g., *Fennel et al.*, 1985]; to provide the additional dissipation, some ions are reflected back upstream by the shock. Those reflected ions are heated by the conversion of some of their ram energy into energy of ion gyration; they are then convected downstream and appear to have been picked up by the flow. Because the ion reflection process is nearly specular [*Gosling and Robson*, 1985], the gyro velocities of the reflected ions should approximate the upstream bulk velocity [*Burgess et al.*, 1995; *Gosling and Robson*, 1985], here the upstream solar wind speed.

The presence of a substantial number of pickup ions at large heliospheric distances means that the environment of the termination shock is fundamentally different from that of the terrestrial bow shock. Reflection of the relatively cold solar wind ions is fundamentally different from the processes by which the relatively energetic pickup ions gain energy at a shock. Using both observations and results of our hybrid simulations, this paper describes a quantitative analysis of solar wind and pickup ion energization at the perpendicular termination shock. Our results are characterized as functions of PUI density ratio ϕ which is defined as the upstream PUI number density over the upstream total number density n_u^{PUI}/n_u. The simulations show that reflected solar wind ions form a PUI-like population; this result helps explain the V2 observations. [*Richardson et al.*, 2008].

Throughout this paper, r_S denotes the shock strength which is also called compression ratio, defined by the density jump n_d/n_u (downstream density over upstream density). The subscript "u" indicates upstream, the subscript "d" indicates downstream. We list V1 and V2 observations in Table 1. In the table, w_s is the shock width which is a few times the ion inertial length and is much larger than the electron inertial length and the ion gyroradius [*Richardson et al.*, 2008]. The quantities u_u and u_d are the bulk velocities upstream and downstream respectively. The quantity θ_{Bn} is the angle between shock normal and the local magnetic field, which is only directly available from V2. The quantity T_d is the downstream temperature (which is also only available from V2) and the temperevealrature jump is expressed as $\tau = T_d/T_u$. Both V1 and V2 observations show that the termination shock is not a strong shock with a shock strength of about 1.6-2.6, and that it is not an effective particle accelerator at the locations in which the Voyagers crossed the shock (i.e., near the nose).

2. Hybrid Plasma Simulations

The Los Alamos Hybrid Plasma Simulation code treats ions as superparticles and electrons as an adiabatic massless fluid [*Winske et al.*, 2003] and thus is ideal for computing ion responses to plasma phenomena (such as the termination shock) at ion length and time scales.

The hybrid code computes the evolution of the plasma quantities as coupled to Maxwell's equations. It solves the following equations self-consistently: 1. Quasi-neutrality $n_e = n_i$; 2. Superparticle ions (here protons) $m_p(dv_p/dt) = e(\overrightarrow{E} + \overrightarrow{v_p} \times \overrightarrow{B}) - e\eta\overrightarrow{J}$; 3. Fluid massless electrons $\partial(n_e m_e \overrightarrow{V_e})/\partial t = -en_e(\overrightarrow{E} + \overrightarrow{V_e} \times \overrightarrow{B}/c) - \nabla \cdot \mathrm{P_e} + en_e \mathrm{R} \cdot \overrightarrow{J}$ where pressure tensor $\mathrm{P_e} = n_e T_e$ and resistivity tensor $\mathrm{R} = \eta \cdot constant$; 4. Maxwell equations (in the low frequency approximation with no displacement current) $\nabla \times \overrightarrow{B} = 4\pi\overrightarrow{J}/c$ and $\nabla \times \overrightarrow{E} = (\partial\overrightarrow{B}/\partial t)/c$ and $\nabla \cdot \overrightarrow{B} = 0$.

Figure 1 illustrate the one dimensional setup for our termination shock simulation. The simulation is run in the downstream rest frame where the stationary shock propagates to the left. The particles are injected from the left wall continuously. The boundary conditions at the right wall (downstream) is set to reflect particles that hit it. Although the simulation is one dimensional in space, its outputs of velocity and magnetic field are fully three dimensional.

We assume that the shock is steady and perpendicular with θ_{Bn} =89.9° in the code. The upstream parameters are chosen to be consistent with the V2 observations. They are: plasma beta β_{sw}=0.05, $u_u = 8v_A$ (or equivalently $M_A = 8$) in the shock frame. We vary the pickup ions density ratios to perform the simulation in different senarios: ϕ =0, 5%, 10%, 12%, 13%, 14%, 15%, 20%, 22%, 25%, 28%, 30%. The solar wind's thermal velocity distribution is assumed to be Maxwellian. The PUIs (if present) velocity distribution is assumed to form a spherical shell at u_u in the frame of the solar wind. Our choice of a shell distribution allows us to distinguish more clearly between the pick ion and the solar wind ion responce to the shock. Further studies, will be needed that model the upstream pickup ions using the *Vasyliunas and Siscoe* [1976] formula, which corresponds to a filled-in velocity distribution. In this study we only consider the conditions near the shock. We do not intend to simulate the foreshock region which extends about 10-15 AU upstream of the shock, nor do we extend our simulations deep into the downstream heliosheath.

2.1. Phase space density

Zero pickup ion case is a baseline computation which provides a comparison against the more realistic cases (with PUIs) to follow. With ϕ =0, the pickup ions are treated as test particles. We separate the directly transmitted solar wind ions from the reflected solar wind ions by flagging ions that propagate backward inside the shock to be reflected ions. However, this method can not separate reflected ions from transmitted ions unambiguously. The reason is that the transmitted ions can also gyrate back and it is hard to tell whether a backward movement inside the shock is due to gyration or reflection. Nevertheless this method provides a qualitative picture of ion reflection. Figure 2 shows a series of phase space density plots from zero pickup ion simulation. The shock is marked by a dash line in Figure 2a and 2b. Both the x, y direction are perpendicular to the magnetic field, which is mostly in the z direction.The upstream solar wind ions form a Maxwellian distribution as assumed. The downstream ions (Figure 2d) are divided into two populations: a heated transmitted solar wind (Figure 2e; core solar wind ions) and a suprathermal tail (Figure 2f; reflected solar wind ions). The figures show that the gyro phases of reflected ions are ~180° off that of the transmitted solar wind ions. Further, the gyro velocity of the reflected ions are approximately equal to the upstream bulk velocity in the shock frame.

Figure 3 presents the phase space density of both the solar wind ions and the pickup ions for the 20% PUI case. Figure 3a shows that solar wind ions behave more uniformly with very few got reflected, as compared to the zero pickup ion case. Figure 3c and Figure 3d are the upstream and downstream solar wind ions respectively. Compared with Figure 2c and Figure 2d, the reflection efficiency of the 20% pickup ion case is significantly reduced. The heating, however, is still very strong. The downstream velocity (Figure 3d) is more than 9 times the upstream velocity ((Figure 3e). On the right hand side, the downstream pickup ions (Figure 3f) are heated slightly more than twice it upstream velocity (Figure 3e). The more quantative result will be calculated in the next subsection.

2.2. Pickup Ion Trajectories

Figure 4 illustrates some velocity-space trajectories of pickup ions from our simulation with pickup ion density ratio of 20%. The panels illustrate the temporal evolution of ions which originate from the same upstream location at the start of the simulation, with one ion per panel. The start time in each is marked with an asterisk, and the color changes from black through blue, green, yellow, orange and red; the last color corresponds to late-time downstream conditions. These trajectories are characteristic of the fraction of pickup ions which gain substantial energy at the shock. The smaller circles with substantial v_x offset correspond to upstream conditions; the larger circles with smaller v_x represent downstream conditions. The transition region (in green) is the part of the trajectory in the vicinity of the shock. Each of these trajectories shows that significant pickup ion energy gain corresponds to particles which encounter the shock with large positive v_x, in contrast to the reflected solar wind ions which correspond to particles with relatively small v_x in the downstream frame. Thus pickup ions are not "reflected" at the shock, but gain energy by a rather different process which is discussed in more detail elsewhere [e.g., *and*; *Winske et al.*, 2009].

2.3. Temperature Jump and Energy Partition

The thermal pressure can be calculated from $P = nkT$, where T is the effective temperature

$$T = \frac{m}{3k}(< v_x^2 - < v_x >^2 > + < v_y^2 - < v_y >^2 > + < v_z^2 - < v_z >^2 >). \qquad (2.1)$$

Here the notation "<>" means to take the average value of the enclosed parameter by averaging it over all the particles from the simulation; m is the mass of a proton; k is the Boltzman constant. Table 2 lists the results from several simulations. In this table, $\frac{n_{PUI}}{n}$ (input column) is the percentage of upstream pickup ions, r_S is the shock strength (density jump), u_d is the downstream velocity written in the unit of *Alfvén* speed v_A. Ideally if all the particles are transmitted, a simple adiabatic heating law with $\gamma = 5/3$ predicts that the temperature jump across a shock should be given by (see Appendix for derivation)

$$\tau_{adiabat} = \frac{T_d}{T_u}|_{adiabat} = r_S^{\gamma-1}. \qquad (2.2)$$

This adiabatic transition has, by definition, no change in entropy across the shock. However, ion reflection is not adiabatic, so the solar wind temperature jump τ_{sw} and the PUI temperature jump τ_{PUI} are both larger than $\tau_{adiabat}$. In particular, the simulation results summarized in Table 2 show $\tau_{sw} >> \tau_{PUI} > \tau_{adiabat}$, which is consistent with the Voyager 2 observations of *Richardson et al.* [2008].

We define η as the percentage of thermal energy that goes into each population

$$\eta_{species} = \frac{P_d^{species} - P_u^{species}}{P_d - P_u}, \tag{2.3}$$

where the species could be PUIs or solar wind. The simulation results of Table 2 show that the net energy gain of PUIs is much greater than that of the solar wind ions (consistent with V2 observation). Another way of looking at energy partition, for easy comparison with Voyager observations, is through the downstream thermal pressure ratio:

$$\chi_d = \frac{P_d^{PUI}}{P_d}, \tag{2.4}$$

χ_d is shown next to the column of η_{PUI} in the table. For the most cases, it approximates η_{PUI}. Thus, the most important conclusions from the hybrid simulation are: (1) the solar wind ions experiences a larger temperature jump, but (2) the PUIs receive a larger portion of the dissipated energy.

3. Rankine-Hugoniot Model

In this section we apply the Rankine-Hugoniot jump conditions to develop a termination shock model with three distinct ion components: transmitted solar wind ions, reflected solar wind ions, and pickup ions. We define two compression parameters, γ and γ_{PUI}, and use these as fitting parameters to enable a comparison of the model predictions against the simulation results.

3.1. Model Equations

Equation 2.2 together with the Rankine-Hugoniot relations ($n_d/n_u = r_S$) and $P = nkT$ give the downstream adiabatic pressure

$$P_d|_{adiabat} = P_u r_S^{\gamma}. \tag{3.1}$$

We emphasis that this condition is a reference quantity associated with no entropy change across the shock.

If we define $\frac{v^2}{3} = \frac{kT}{m}$ with v corresponding to an average particle thermal speed in the solar wind frame, then

$$P = \rho v^2/3 \tag{3.2}$$

where ρ is mass density. This means that

$$P_u^{sw} = \rho_{sw} v_{sw,u}^2/3, \tag{3.3}$$

and that

$$P_u^{PUI} = \rho_{PUI} v_{PUI,u}^2/3 = \phi \rho_u u_u^2/3, \tag{3.4}$$

where $v_{sw,u}$ is the thermal velocity of the solar wind; ϕ is the upstream PUI density ratio as previously defined. The average PUI upstream thermal velocity is assumed to be the upstream bulk velocity as the pickup process implied, and also to be consistent with the shell distribution used in the simulations.

Both the Voyager 2 observations and our hybrid simulations show that the downstream pickup ions gain more energy than would be predicted by the adiabatic equation 3.1 with $\gamma = 5/3$. To represent this in our model, we assume that downstream of the shock the thermalization of PUI follows equation 3.1 but with a γ which is considered a fitting parameter greater than 5/3:

$$P_d^{PUI} \simeq r_S^{\gamma_{PUI}} P_u^{PUI}; \tag{3.5}$$

Equation 3.4 and 3.5 together give

$$P_d^{PUI} = r_S^{\gamma_{PUI}} \phi \rho_u u_u^2/3 \tag{3.6}$$

It can be derived, from the simulations, that γ_{PUI} is approximately 2.3 on average. The simulations further show that, even with pickup ions, some solar wind ions are specularly reflected at the shock. So, in this model, we assume the solar wind ions can be divided into two parts: a transmitted component and a reflected component. Let ϵ_{ref} be the reflection efficiency of the solar wind ions: the number density of reflected solar wind ions divided by the number density of the solar wind ions. Then the transmitted solar wind population has a downstream pressure of

$$P_d^{sw-trans} = r_S^{\gamma} P_u^{sw-trans} = r_S^{\gamma}(1-\epsilon_{ref})P_u^{sw}, \tag{3.7}$$

where the superscripts "ref" and "sw-trans" represent "reflected ions" and "solar wind transmitted ions (core population)" respectively. The upstream solar wind pressure can be expressed as

$$P_u^{sw} = P_u - P_u^{PUI} = P_u - \phi \rho_u u_u^2/3, \tag{3.8}$$

where we made used of equation 3.4. Equation 3.7 and 3.8 give

$$P_d^{sw-trans} = r_S^{\gamma}(1-\epsilon_{ref})(P_u - \phi\rho_u u_u^2/3), \tag{3.9}$$

As we see from simulation in §2.1, in the downstream flow frame the reflected ions have a thermal velocity of $v_d^{sw-ref} \simeq \sqrt{2}u_u$ because of specular reflection. With equation 3.2, we then find that

$$P_d^{sw-ref} = \rho_d^{sw-ref}(v_d^{sw-ref})^2/3 = (\epsilon_{ref}(1-\phi)\rho_d)2u_u^2/3 = 2r_S\epsilon_{ref}(1-\phi)\rho_u u_u^2/3. \tag{3.10}$$

The total downstream pressure can be expressed as the sum of the transmitted solar wind thermal pressure, the reflected solar wind thermal pressure and the transmitted PUI thermal pressure

$$P_d = P_d^{sw-trans} + P_d^{sw-ref} + P_d^{PUI}. \qquad (3.11)$$

Using equation 3.6, 3.9 and 3.10, we can rewrite the above equation as,

$$P_d = r_S^{\gamma}(1-\epsilon_{ref})(P_u - \phi\rho_u u_u^2/3) + 2r_S\epsilon_{ref}(1-\phi)\rho_u u_u^2/3 + r_S^{\gamma_{PUI}}\phi\rho_u u_u^2/3. \qquad (3.12)$$

Conservation of momentum across the shock (Appendix equation A.8) requires that

$$\rho_u u_u^2 + P_u + \frac{B_u^2}{2\mu_0} = \rho_d u_d^2 + P_d + \frac{B_d^2}{2\mu_0} \qquad (3.13)$$

Substitute P_d with equation 3.12 and B_d with equation A.10 (Appendix), we get

$$\rho_u u_u^2 + P_u + \frac{B_u^2}{2\mu_0} = \rho_d u_d^2 + r_S^{\gamma}(1-\epsilon_{ref})(P_u - \phi\rho_u u_u^2/3) + 2r_S\epsilon_{ref}(1-\phi)\rho_u u_u^2/3 + r_S^{\gamma_{PUI}}\phi\rho_u u_u^2/3 + \frac{r_S^2 B_u^2}{2\mu_0}. \qquad (3.14)$$

Divided equation 3.14 by $\rho_u u_u^2$ and solve for ϵ_{ref}

$$\epsilon_{ref} = \frac{1 - \frac{1}{r_S} + \frac{1-r_S^2}{2M_A^2} + (1-r_S)\delta + \frac{\phi}{3}(r_S^{\gamma} - r_S^{\gamma_{PUI}})}{\frac{2r_S(1-\phi)}{3} + \frac{r_S^{\gamma}\phi}{3} - r_S^{\gamma}\delta} \qquad (3.15)$$

where *Alfvénic* mach number $M_A = (\frac{\mu_0\rho_u u_u^2}{B_u^2})^{1/2}$ and $\delta = P_u/(\rho_u u_u^2) = (P_u^{sw} + P_u^{PUI})/(\rho_u u_u^2)$. For given upstream solar wind beta β_{sw} and M_A, δ can be expressed as

$$\delta = \frac{P_u}{\rho_u u_u^2} = \frac{P_u^{sw} + P_u^{PUI}}{\rho_u u_u^2} \qquad (3.16)$$

173 where we make use of equation 3.3, 3.4, and that solar wind plasma beta $\beta_{sw} = \frac{2v_{sw,u}^2 M_A^2}{3v_u^2}$.

So with given upstream solar wind beta β_{sw} and *Alfvénic* Mach number M_A and specific heats γ, γ_{PUI} for any chosen PUIs ratio ϕ, we can calculate δ and sonic Mach number

$$M_{cs}^2 = 1/(\gamma\delta). \qquad (3.17)$$

With the above equation, equation A.11 (Appendix) can be rewritten as

$$(r_S - 1)[r_S^2\frac{2-\gamma}{M_A^2} + r_S(\frac{\gamma}{M_A^2} + 2\gamma\delta + \gamma - 1) - (\gamma+1)] = 0 \qquad (3.18)$$

We can then solve for shock strength r_S from equation 3.18 and solar wind reflection efficiency ϵ_{ref} using equation 3.15.

The thermal pressure jump can be derived to be

$$\frac{P_d}{P_u} = r_S^\gamma(1-\epsilon_{ref})(1-\frac{\phi}{3\delta}) + \frac{2r_S\epsilon_{ref}(1-\phi)}{3\delta} + \frac{r_S^{\gamma_{PUI}}\phi}{3\delta}, \qquad (3.19)$$

and the downstream pickup ions thermal pressure ratio is

$$\chi_d = \frac{P_d^{PUI}}{P_u} = \frac{r_S^{\gamma_{PUI}}\phi}{r_S^\gamma(1-\epsilon_{ref})(3\delta-\phi) + 2r_S\epsilon_{ref}(1-\phi) + r_S^{\gamma_{PUI}}\phi}. \qquad (3.20)$$

In order to compare our model results with Voyager observations and our hybrid simulations, we choose the same values of $M_A = 8$, $\beta_{sw} = 0.05$ as the previous section. We also specify $\gamma_{PUI} = 2.3$ (empirically derived from simulation using equation 3.6). Figure 5 shows model results for r_S, P_d/P_u, and P_d^{PUI}/P_d as functions of the pickup ion density ratio for the choice of two different values of γ. Values of the pickup ion energy fraction from the simulation are shown as diamonds. Both the r_S and P_d^{PUI}/P_d panels demonstrate that with the increase of PUI ratio ϕ, the simulated values trend from the γ=5/3 curve toward the γ=2.05 curve. This tendency is not as obvious as in the P_d/P_u panel because the two curves are rather close. Overall, the results from our analytic model are consistent with the simulations. The V2 observed P_d^{PUI}/P_d of approximately 80% corresponds to a PUI density ratio of 10.5% (for γ=5/3) or 22.0% (γ=2.05).

In Figure 6, ϵ_{ref} is plotted in black as a function of ϕ. The dash line corresponds to a γ of 5/3. From 0% PUI to 20% PUI, the reflection efficiency ϵ_{ref} drops dramatically to zero. If γ=2.05, the reflection efficiency of solar wind ions is very low for all values of pickup ion density ratio.

3.2. Energy Partition during Dissipation

The percentage of heating that goes to the transmitted solar wind ions can be derived from equation 2.4

$$\eta_{sw-trans} = \frac{(1-\epsilon_{ref})(r_S^{\gamma}-1)(\delta-\phi/3)}{r_S^{\gamma_{PUI}}\phi/3 + r_S^{\gamma}(\delta-\phi/3)(1-\epsilon_{ref}) + 2\epsilon_{ref}r_S(1-\phi)/3-\delta}. \tag{3.21}$$

Similarly, the percentage of heating that goes to reflected solar wind ions and PUIs respectively are

$$\eta_{sw-ref} = \frac{2\epsilon_{ref}r_S(1-\phi)/3 - \epsilon_{ref}(\delta-\phi/3)}{r_S^{\gamma_{PUI}}\phi/3 + r_S^{\gamma}(\delta-\phi/3)(1-\epsilon_{ref}) + 2\epsilon_{ref}r_S(1-\phi)/3-\delta}, \tag{3.22}$$

$$\eta_{PUI} = \frac{\phi(r_S^{\gamma}-1)/3}{r_S^{\gamma_{PUI}}\phi/3 + r_S^{\gamma}(\delta-\phi/3)(1-\epsilon_{ref}) + 2\epsilon_{ref}r_S(1-\phi)/3-\delta}. \tag{3.23}$$

The two parameters η_{sw-ref} and η_{PUI} are plotted in Figure 5 in blue and red respectively. The percentage of heating that goes to the transmitted solar wind ions $\eta_{sw-trans}$ is neglegibly small and thus is not shown. The percentage of heating that goes to pickup ions η_{PUI} increases with increasing PUI density ratio ϕ. The percentage of heating that goes to the reflected solar wind ions η_{sw-ref} decrease with increasing ϕ. Below 7.5% (for γ=2.05) or 12.5% (for γ=5/3) PUI, $\eta_{sw-ref} > \eta_{PUI}$ (which is the case of *Liewer et al.* [1993]'s simulation), above these values, $\eta_{sw-ref} < \eta_{PUI}$ (which is the case V2 measured). We further overplot η_{PUI} from our simulation in red diamonds. Again, with the increase of PUI ratio, the simulated values trends toward the γ=2.05 curve.

3.3. The Gas Kinetic Character of the Termination Shock

The downstream *Alfvénic* mach number can be obtained analytically with the aid of equation A.10 (Appendix)

$$M_{A,d} = \frac{u_d}{v_{A,d}} = u_d\left(\frac{\mu_0\rho_d}{B_d^2}\right)^{1/2} = r_S^{-1.5}u_u\left(\frac{\mu_0\rho_u}{B_u^2}\right)^{1/2} = r_S^{-1.5}M_A. \tag{3.24}$$

With the upstream *Alfvénic* mach number $M_A = 8$, for the pickup ion ratio ϕ=[0, 30%], $M_{A,d}$=[1.11, 1.95] (for γ=5/3) or $M_{A,d}$=[1.63, 2.67] (for γ=2.05). This means that downstream of shock, the flow is still super *Alfvénic*, which is consistent with V2 observation by *Li et al.* [2008].

The downstream sonic Mach number can also be obtained analytically

$$M_{cs,d} = \frac{u_d}{v_{cs}} = u_d(\frac{\rho_d}{\gamma P_d})^{1/2} = \frac{M_{cs}}{\sqrt{r_S P_d/P_u}}, \tag{3.25}$$

where the upstream $M_{cs} = 1/(\gamma\delta)$ can be calculated as have been discussed before. The pressure jump P_d/P_u is known from equation 3.19. For the pickup ion ratio ϕ=[0, 30%], $M_{cs,d}$=[0.50, 0.59] (for γ=5/3) or $M_{cs,d}$=[0.54, 0.63] (for γ=2.05).

The magnetosonic Mach number M_{MS} [*Cravens*, 1997] is defined as the coupled Mach number of *Alfvénic* mach number M_A and sonic mach number M_{cs}

$$M_{MS} = \frac{u}{\sqrt{v_A^2 + v_{cs}^2}} = \frac{M_A M_{cs}}{\sqrt{M_A^2 + M_{cs}^2}} \tag{3.26}$$

For all of our simulations, the downstream magnetosonic Mach number falls within the range of [0.57, 0.45] (for γ=5/3) or [0.51, 0.62] (for γ=2.05). All the theoretically calculated mach numbers are plotted in Figure 7 for immediate visionazition. Although the downstream flow is super *Alfvénic*, it is still subsonic and sub-magnetosonic. The shock has more of a character of a gas kinetic shock than a *Alfvénic* shock as oppose to the planetary bow shocks, due to the participation of PUIs in the shock dynamics.

4. Discussion

Pickup ions gain more net energy because they have a much larger upstream thermal energy than the solar wind ions. Even if solar wind ions are preferred for reflection and gain a relatively large increase in temperature, their net energy gain remains small compared to the energy increase of the pickup ions. In summary, for all parameters considered here,

$$\tau_{sw} >> \tau_{PUI}, \tag{4.1}$$

and for sufficiently large n_{PUI}/n,

$$\eta_{PUI} >> \eta_{sw} \tag{4.2}$$

In a sense, *Liewer et al.* [1993] and *Richardson et al.* [2008] are both right on heating and energy partition respectively.

As we see from the comparision between the simulations and the theoretical results. As we increase the pickup ions ratio, a γ of 2 describes the PUI energization bettter than a γ of 5/3. More of the energization process will be discuss in the *Winske et al.* [2009] paper.

In this paper's derivation we neglect the dissipation by the magnetic field and instabilities. The reason we can do this is because the magnetosonic mach number M_{MS} is a lot more closer to the sonic mach number M_{cs} than to the *Alfvénic* mach number M_A for the termination shock. This hints that the gas kinetic character of the termination shock dominates over its *Alfvénic* character. The PUIs' presence gives the termination shock the properties of a weak gas kinetic shock (as differs from the Earth's bow shock- strong *Alfvénic* shock) however with ion reflection. In this paper we also neglect resistivity, which should be small because the plasma is collisionless within the termination shock's length scale.

5. Concluding Remarks

We have used the one-dimensional Los Alamos hybrid code to carry out a series of simulations of the perpendicular termination shock in the presence of both solar wind ions and pickup ions. We have also developed an analytic model for the response of both ion components at such a shock. The existence of the PUIs reduces the shock as expected. The PUIs enhance the effective plasma beta upstream and weaken the magnetosonic mach number.

Both the simulations and the model show that, although the presence of the pickup ions weakens the shock, it remains supercritical, which means that some of the upstream solar wind ions are reflected in order to achieve the dissipation necessary to slow the flow. The reflected solar wind ions gain a gyrotropic speed of the order of the upstream flow speed, and then are swept downstream. This gives some solar wind ions the same order of magnitude kinetic energy as the pick-up ions, so that it is very difficult to observationally separate solar wind ions from pick-up ions downstream.

The simulations further show that, although the pickup ion energy gain is greater than predicted by adiabatic compression, the picture of specular reflection, appropriate for the relatively cold solar wind ions, is not applicable to the relatively warm pickup ions. Rather than a simple reversal of the v_x velocity as in reflection, both the v_x and v_y velocity components play a role in the transfer of energy to the pickup ions. Further discussion of this topic is beyond the scope of this paper; see *Winske et al.* [2009] for a more detailed discussion of the physics.

We have derived an analytic model based on the Rankine-Hugoniot jump conditions with fitting parameters derived from our hybrid simulations to compute the relative energy gain at a perpendicular shock for three components: transmitted solar wind ions, reflected solar wind ions, and pick-up ions. The results are in good agreement with our simulations and are consistent with the limited plasma observations of V2 at the termination shock. We find that when the PUI ratio is more than about 10% (depends on γ), more energy goes to heat up pickup ions than reflected solar wind ions ($\eta_{PUI} > \eta_{sw-ref}$). The reason is that PUIs start with a much larger initial thermal energies. Only when the PUI ratio is less than 10%, more energy goes to heat up the reflected solar wind ions than the PUIs

($\eta_{sw-ref} > \eta_{PUI}$) and the solar wind dominates the dissipation, which is the case of the *Liewer et al.* [1993] study. Our result support *Richardson et al.* [2008]'s claim that much of the dissipation goes to PUIs as well as *Liewer et al.* [1993]'s claim that solar wind ions are heated more. We also made prediction that the PUI ratio at the termination shock is about 10.5-22%.

Instead of a strong *Alfvénic* shock, e.g., the earth bow shock that we are familiar with, the termination shock behaves more like a gas kinetic shock (because of the PUIs) with the addition of ion reflection.

Appendix A

Starting with adiabatic law

$$PV^{\gamma} = constant, \tag{A.1}$$

where $P = nkT \propto nkv^2$ and $V \propto 1/n$, so

$$nv^2(1/n)^{\gamma} = v^2/n^{\gamma-1} = constant. \tag{A.2}$$

With upstream and downstream conditions, the above equation turns into

$$v_u^2/n_u^{\gamma-1} = v_d^2/n_d^{\gamma-1}. \tag{A.3}$$

Substitute shock strength $r_S = n_d/n_u$ into it, we arrive at

$$v_d = v_u(r_S)^{(\gamma-1)/2}. \tag{A.4}$$

Define temperature jump for transmitted ion $\tau_{adiabat}$,

$$\tau_{adiabat} = \frac{T_d}{T_u} = (v_d/v_u)^2 = (r_S)^{\gamma-1} \tag{A.5}$$

The Rankine-Hugoniot relations for a perpendicular shock are derived in the frame of a steady shock. Both upstream and downstream plasma are assumed to satisfy the equations of ideal MHD. The resulting equations are [*Burgess et al.*, 1995]:

- 1. Conservation of mass

$$[\rho u] = 0; \tag{A.6}$$

- 2. Continuity of tangential electric field

$$[uB] = 0; \tag{A.7}$$

- 3. Conservation of momentum

$$[\rho u^2 + P + \frac{B^2}{2\mu_0}] = 0; \tag{A.8}$$

- 4. Conservation of energy

$$[\rho u(\frac{1}{2}u^2 + \frac{\gamma}{\gamma - 1}\frac{P}{\rho}) + u\frac{B^2}{\mu_0}] = 0. \tag{A.9}$$

The shock strength r_S is defined as the shock jump of velocity, density and magnetic field (for perpendicular shocks)

$$r_S = \frac{u_u}{u_d} = \frac{\rho_d}{\rho_u} = \frac{B_d}{B_u}. \tag{A.10}$$

Combining A.6-A.10, we find [*Burgess et al.*, 1995]:

$$(r_S - 1)[r_S^2\frac{2-\gamma}{M_A^2} + r_S(\frac{\gamma}{M_A^2} + \frac{2}{M_{cs}^2} + \gamma - 1) - (\gamma + 1)] = 0, \tag{A.11}$$

where $M_A = u_u(\mu_0\rho_u)^{1/2}/B_u$ is the *Alfvénic* mach number; $M_{cs} = u_u(\rho_u/\gamma P_u)^{1/2}$ is the sonic mach number.

Acknowledgments. The authors thank Gary Zank and Sandra Chapman for very extensive and very helpful discussions. The Los Alamos portion of this work was performed under the auspices of the U.S. Department of Energy (DOE), and was supported by the Solar and Heliospheric Physics SR&T Program of the National Aeronautics and Space Administration. This Boston University portion is funded by the IBEX mission.

References

and, M. A. L. ().

Burgess, D., M. G. Kivelson, and C. T. Russell (1995), Introduction to space physics, *Cambridge University Press*, pp. 129–163.

Burlaga, L. F., N. F. NESS, M. H. Acuna, R. P. Lepping, J. E. Connerney, E. C. Stone, and F. B. McDonald (2005), Crossing the termination shock into the heliosheath: Magnetic fields, *Science*, *309*, 2027.

Cravens, T. E. (1997), Physics of solar system plasmas, *Cambridge University Press*, p. 134.

Decker, R. B., S. M. Krimigis, E. C. Roelof, M. E. Hill, T. P. Armstrong, G. Gloeckler, D. C. Hamilton, and L. J. Lanzerotti (2005), Voyager 1 in the foreshock, termination shock, and heliosheath, *Science*, *309*, 2020.

Decker, R. B., S. M. Krimigis, E. C. Roelof, M. E. Hill, T. P. Armstrong, G. Gloeckler, D. C. Hamilton, and L. J. lanzerotti (2008), Mediation of the solar wind termination shock by non-thermal ions, *Nature*, *454*, 67–70.

Fennel, C. F., J. P. Edmiston, and T. Hada (1985), A quarter century of collionless shock research, *Geophysical Monograph*, *34*.

Goodrich, C. C. (1985), Numerical simulations of quasi-perpendicular collisionless shock, *Geophysical Monograph*, *35*, 153–168.

Gosling, J. T., and A. E. Robson (1985), Ion reflection, gyration, and dissipation at supercritical shocks, *Geophysical Monograph*, *35*, 141–152.

Li, H., C. Wang, and J. D. Richardson (2008), Properties of the termination shock observed by voyager 2, *Geophys. Res. Lett.*, *35*, L19,107.

Liewer, P. C., B. E. Goldstein, and N. Omidi (1993), Hybrid simulations of the effects of interstellar pickup hydrogen on the solar wind termination shock, *J. Geophys. Res.*, *98*, 15,211.

Paschmann, G., N. Sckopke, S. J. Bame, and J. T. Gosling (1982), Observations of gyrating ions in the foot of the nearly perpendicular bow shock, *Geophys. Res. Lett.*, *9*, 881.

Phillips, P. E., and A. E. Robson (1972), Influence of reflected ions on the magnetic structure of a collionless shock front, *Phys. Rev. Lett.*, *29*, 154.

Quest, K. B. (1985), Simulation of high-mach-number collisionless perpendicular shock in astrophysical plasmas, *Physical Review*, *54*, 16.

Richardson, J. D., J. C. Kasper, C. Wang, J. W. Belcher, and A. J. Lazarus (2008), Cool heliosheath plasma and deceleration of the upstream solar wind at the termination shock, *Nature.*

Sckopke, N., G. Paschmann, S. J. Bame, and J. T. Gosling (1983), Evolution of ion distribution across the nearly perpendicular bow shock: specularly and non-specularly reflected-gyrating ions, *J. Geophys. Res.*, *88*, 6121–6136.

Stone, E. C., A. C. Cummings, F. B. McDonald, B. C. Heikkila, N. Lal, and W. R. Webber (2005), Self-consistent hybrid simulations of the interaction of the heliosphere with the local interstellar medium, *Science*, *309*, 2017.

Vasyliunas, V. M., and G. L. Siscoe (1976), On the flux and energy spectrum of interstellar ions in the heliosphere, *J. Geophys. Res.*, *81*, 1247.

Winske, D., J. T. Gosling, and M. F. Thomsen (1986), Comments on "increase of ion kinetic temperature across a collisionless shock: I. a new concept by l. c. lee et al." and "ion acceleration in quasiperpendicular magnetosonic shock waves with subcritical mach number by y. ohsawa and j. sakai", *Geophys. Res. Lett.*, *13*, 561–562.

Winske, D., L. Yin, N. Omidi, H. Karimabadi, and K. B. Quest (2003), Self-consistent hybrid simulations of the interaction of the heliosphere with the local interstellar medium, *edited by J. Buechener, C.T.Dum and M. Scholer, Springer Verlag.*, pp. 140–169.

Winske, D., S. P. Gary, P. Wu, and N. A. Schwadron (2009), Pick-up ion energization at the termination shock, *Geophys. Res. Lett.*, *submitted.*

Woods, L. C. (1969), Critical alfven mach numbers for transverse field mhd shocks, *Plasma Physics*, *11*, 25.

Zank, G. P., H. L. Pauls, I. H. Cairns, and G. M. Webb (1996), Interstellar pickup ions and quasi-perpendicular shocks: Implications for the termination shock and interplanetary shocks, *J. Geophys. Res.*, *101*, 457–477.

Table 1. Voyager 1 (V1) and Voyager 2 (V2) Termination Shock Encounters

encounters	$r(AU)$	r_S	u_u (km/s)	u_d (km/s)	θ_{Bn}	w_s (km)	τ	T_d (k)
V1	94	$2.6^{+0.4}_{-0.2}$	200	100	-	-	-	-
$V2(TS-2)$	84	2.38 ± 0.14	325	150	$82.8° \pm 3.9°$	300,300	10	10^5
$V2(TS-3)$	84	1.58 ± 0.71	250	150	$74.3° \pm 11.2°$	100,000	10	10^5

[*Richardson et al.*, 2008; *Stone et al.*, 2005; *Decker et al.*, 2005; *Burlaga et al.*, 2005]

TS-2 is the 2nd termination shock crossing when the termination shock is moving outwards, and TS-3 is the 3rd termination shock crossing when the termination shock is moving inwards. The quantity w_s is the shock width; and the quantity $\tau = \frac{T_d}{T_u}$ is the temperature jump.

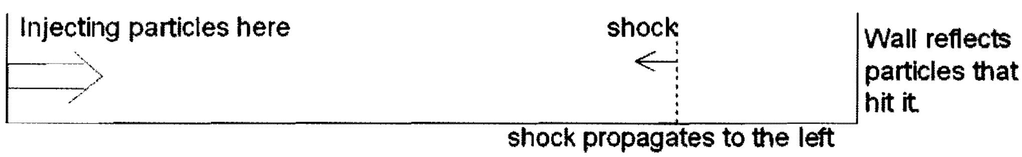

Figure 1. One-dimensional setup for the termination shock simulation

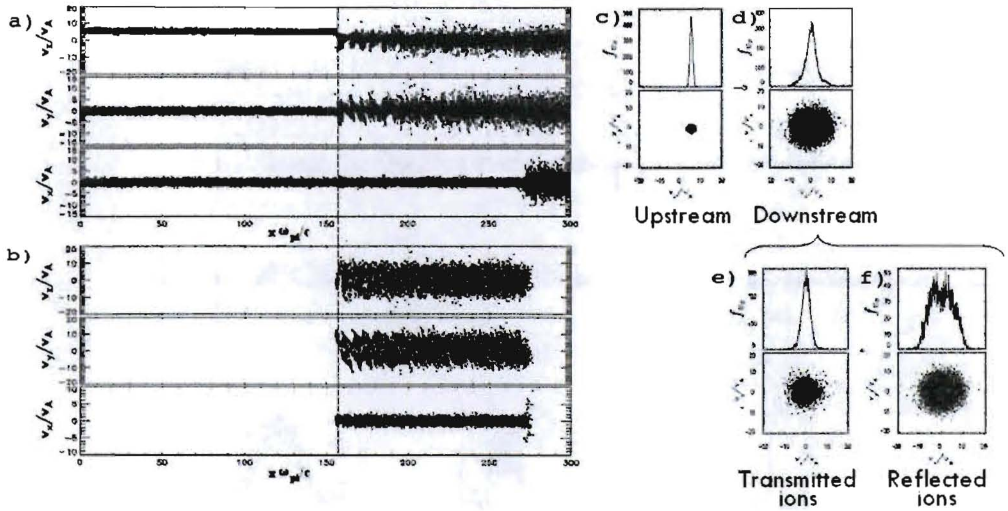

Figure 2. Phase space density of case 1 (no PUIs) in the downstream rest frame. a. Transmitted (core) solar wind ions. b) Reflected solar wind ions. The shock is marked by a dash line. c) Upstream phase space density. d) Downstream phase space density. e) Downstream transmitted (core) solar wind ions. f) Downstream reflected solar wind ions. So c) becomes d) after the shock. And d)=e)+f).

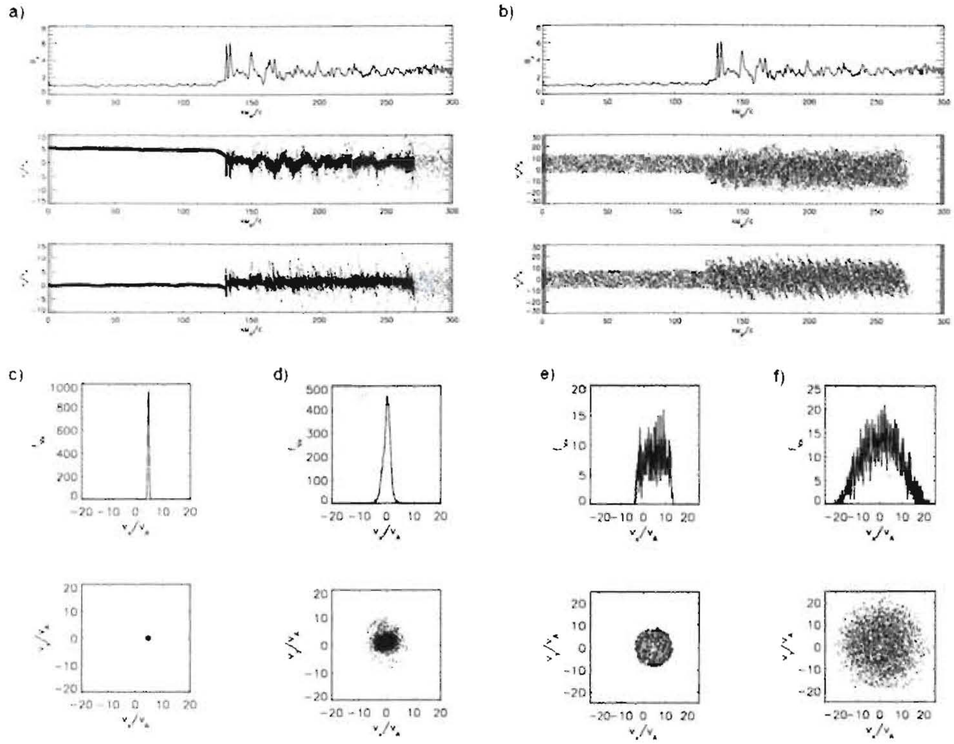

Figure 3. Phase space density of case 4 (20%) in code units in the downstream rest frame. Solar wind ions are plotted in the panels on the left and pickup ions are plotted in the panels on the right. a) Upstream and downstream solar wind ions. b) Upstream and downstream pickup ions. c) Upstream solar wind ions. d) Downstream solar wind ions. e) Upstream pickup ions. f) Downstream pickup ions.

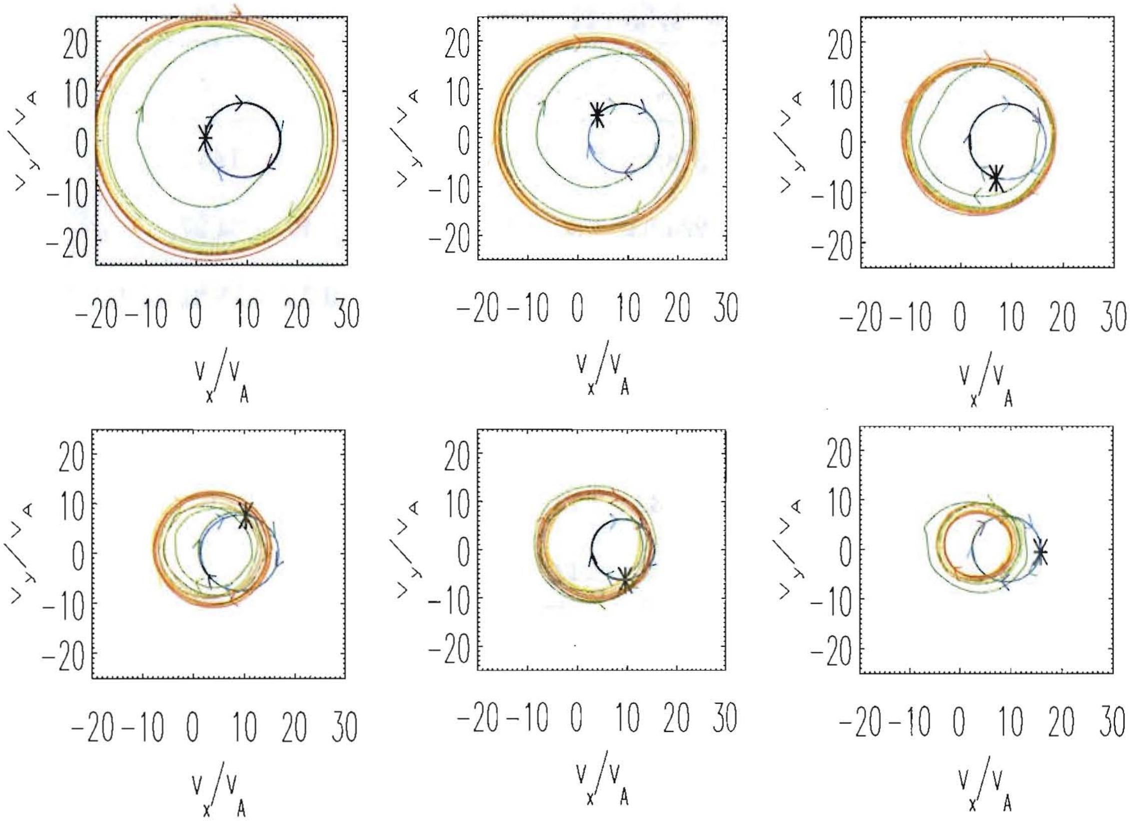

Figure 4. PUIs trajectories in velocity space (in the shock frame), with both v_x and v_y in the unit of v_A. Each panel is a particle trajectory from time zero to time end of the simulation. Time zero is marked by an asterisk. The arrows mark the directions of the trajectories. From time zero to time end, the trajectory's color changes from black through blue, green, yellow, orange and red.

Table 2. Results Calculated from the Hybrid Simulation ($M_A = 8$, $\beta_{sw} = 0.05$)

n_u^{PUI}/n_u	$u_d(v_A)$	$r_S = \frac{n_d}{n_u}$	$\tau_{adiabat}$	τ_{sw}	τ_{PUI}	η_{sw}	η_{PUI}	$\frac{P_d^{PUI}}{P_d}$	$\chi_d = \frac{P_d}{P_u}$
0%	1.80	4.06	2.04	378.46	5.85	100%	-	-	1451
5%	2.14	3.46	1.97	224.63	4.96	55.7%	44.3%	0.49	34.27
10%	2.25	3.14	1.85	102.57	3.53	34.8%	55.2%	0.71	15.81
15%	2.66	2.70	1.72	52.17	3.30	20.4%	79.6%	0.85	10.55
20%	3.04	2.32	1.62	14.69	2.46	13.2%	86.8%	0.91	6.19
25%	3.17	2.12	1.55	26.32	2.43	15.4%	84.6%	0.87	6.01
30%	3.55	2.04	1.55	8.14	2.42	13.0%	87.0%	0.90	5.61

Here energy partition $\eta_{species} = \frac{P_d^{species} - P_u^{species}}{P_d - P_u}$, temperature jump $\tau_{species} = \frac{T_d^{species}}{T_u^{species}}$.

Table is explained in detail in §2.3.

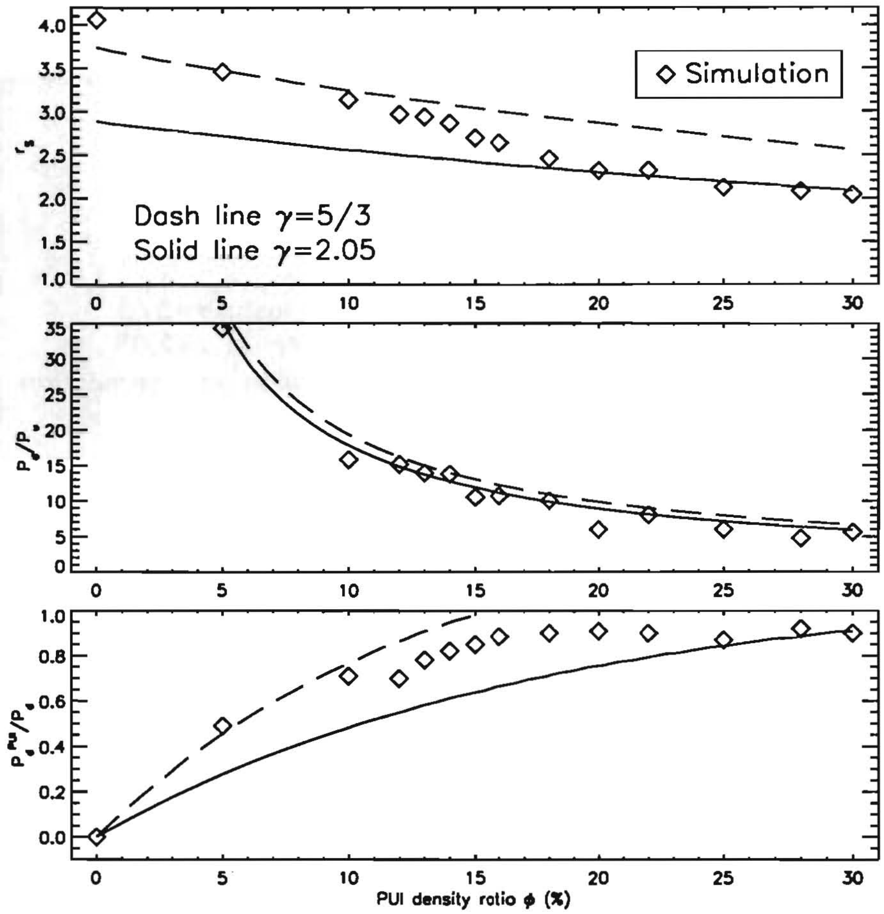

Figure 5. Compression ratio r_S, pressure jump P_d/P_u and downstream pickup ions thermal pressure ratio P_d^{PUI}/P_d are plotted as a function of pickup ion density ratio ϕ. Dash lines are the theoretical prediction when γ is set to be 5/3, the solid lines are when γ is 2.05. The diamonds are values from simulations.

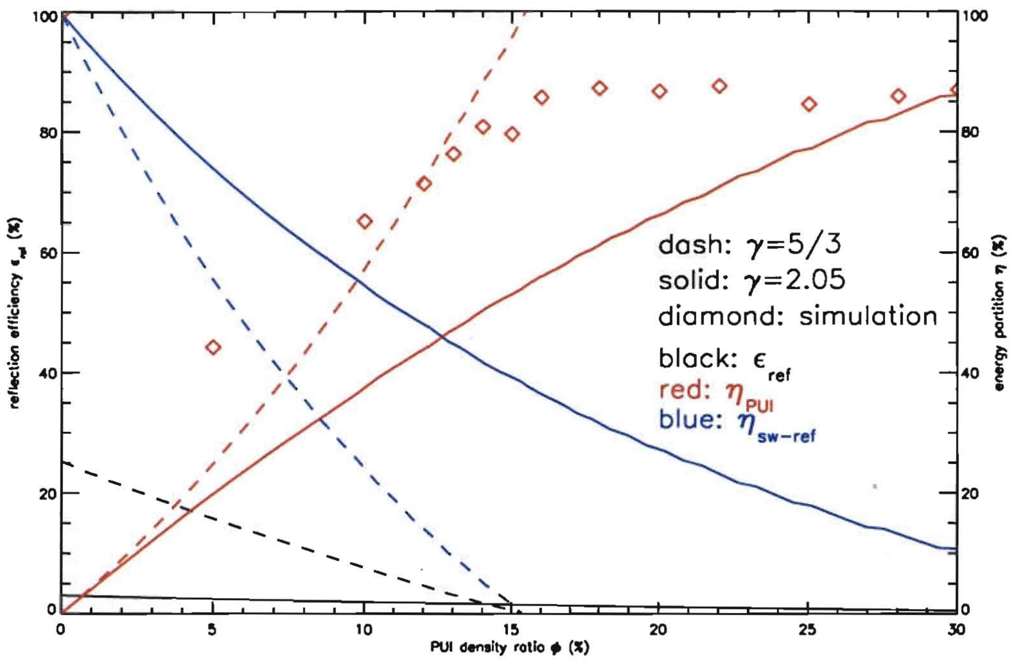

Figure 6. Reflection efficiency ϵ_{ref} (%) and energy partition η (%) as a function of PUI ratio ϕ. Red diamonds are the percentage of heating the PUIs gain from the simulations.

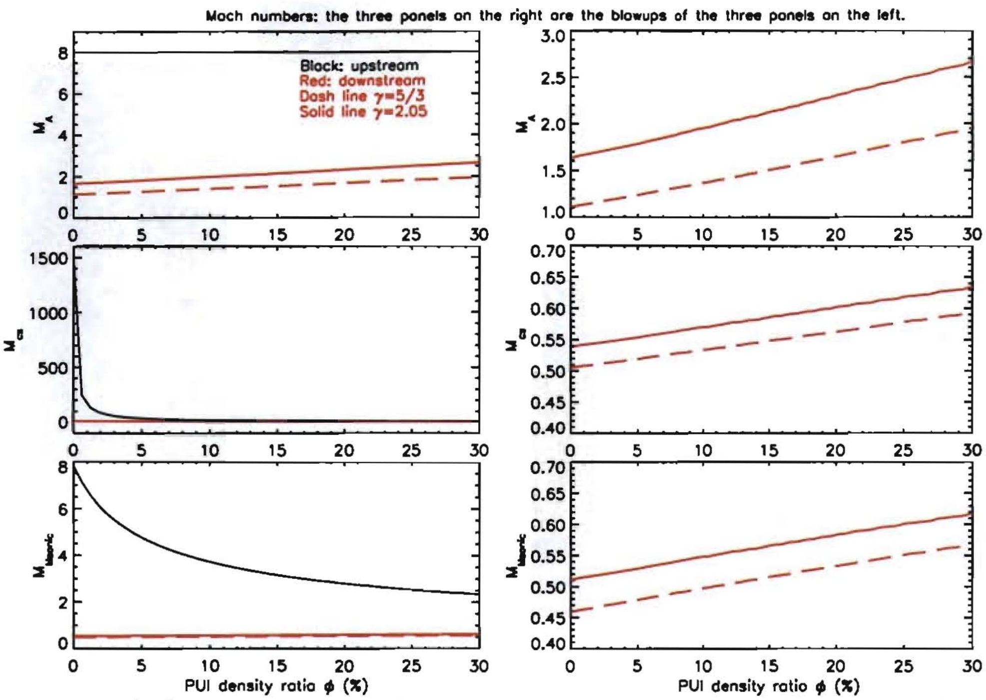

Figure 7. Mach numbers: The three panels on the right are the blowups of the same quantities of the three panels on the left: top panel *Alfvénic* mach number M_A, middle panel sonic mach number M_cs, bottom panel Magnetosonic mach number $M_M sonic$. In the blow up panels, we can have a better view of how the solid red lines differ from te dash lines. The black lines are the upstream mach numbers as a function of pickup ion ratio ϕ; the red lines are the theoretically calculated downstream mach numbers at γ=5/3 and the red dash lines are the theoretically calculated downstream mach numbers at γ=2.05.